ADVANCED ENERGY MATERIALS
www.advenergymat.de

A Novel Phase of $Li_{15}Si_4$ Synthesized under Pressure

Zhidan Zeng, Qingfeng Zeng, Nian Liu, Artem R. Oganov, Qiaoshi Zeng, Yi Cui, and Wendy L. Mao**

$Li_{15}Si_4$, the only crystalline phase that forms during lithiation of the Si anode in lithium-ion batteries, is found to undergo a structural transition to a new phase at 7 GPa. Despite the large unit cell of $Li_{15}Si_4$ (152 atoms in the unit cell), ab initio evolutionary metadynamics (using the USPEX code) successfully predicts the atomic structure of this new phase (β-$Li_{15}Si_4$), which has an orthorhombic structure with an *Fdd2* space group. In the new β-$Li_{15}Si_4$ phase Si atoms are isolated by Li atoms analogous to the original cubic phase (α-$Li_{15}Si_4$), whereas the atomic packing is more efficient owing to the higher Si—Li coordination number and shorter Si—Li, Li—Li bonds. β-$Li_{15}Si_4$ has substantially larger elastic moduli compared with α-$Li_{15}Si_4$, and has a good electrical conductivity. As a result, β-$Li_{15}Si_4$ has superior resistance to deformation and fracture under stress. The theoretical volume expansion of Si would decrease 25% if it transforms to β-$Li_{15}Si_4$, instead of α-$Li_{15}Si_4$, during lithiation. Moreover, β-$Li_{15}Si_4$ can be recovered back to ambient pressure, providing opportunities to further investigate its properties and potential applications.

1. Introduction

The Li–Si system has attracted great attention for its promising energy storage applications, particularly because Si as an anode material for Li-ion batteries has the highest theoretical capacity, low discharge potential (vs Li/Li^+), and is abundant in the Earth.[1,2] The Li–Si system has a rich phase diagram with many well-known intermediate compounds, e.g., $Li_{12}Si_7$, Li_7Si_3, $Li_{13}Si_4$, $Li_{21}Si_5$, and recently discovered $Li_{16.42}Si_4$ and $Li_{17}Si_4$.[3,4] Owing to its technical importance, numerous experimental and theoretical studies have been carried out to understand the structure, stability, and mechanical and electrical properties of phases in this system.[5–9] Li–Si compounds were also directly used as prelithiated anode materials.[10,11] However, in situ X-ray diffraction (XRD) studies on the lithiation /delithiation of Si anodes confirmed the absence of the above-mentioned stable compounds in the electrochemical reaction in Li-ion batteries at room temperature.[12,13] The only crystalline lithium silicide formed is $Li_{15}Si_4$ (space group $I\bar{4}3d$), a metastable phase that decomposes to $Li_{13}Si_4$, $Li_{17}Si_4/Li_{4.11}Si$, or amorphous/weakly crystalline products when annealed at temperatures above 200 °C.[12–14] In order to optimize the performance of Si anodes, properties of $Li_{15}Si_4$ have been investigated extensively by theoretical simulations.[6,15] At the same time, experimental study has proven to be difficult partially because of the challenges associated with material synthesis and handling due to its high reactivity.[7,14]

As an anode material, one critical issue Si encounters is the significant internal stress (of the order of magnitude of GPa) built up during Li insertion, resulting in severe electrode fracture and capacity decay.[16–18] Significant effort has been devoted

Dr. Z. Zeng, Dr. Q. S. Zeng, Prof. W. L. Mao
Department of Geological Sciences
Stanford University
Stanford, CA 94305, USA
E-mail: zengzd@hpstar.ac.cn; wmao@stanford.edu
Dr. Z. Zeng, Dr. Q. S. Zeng
Center for High Pressure Science and
Technology Advanced Research (HPSTAR)
Shanghai 201203, China
Prof. Q. F. Zeng
Science and Technology on Thermostructural
Composite Materials Laboratory
International Center for Materials Discovery
School of Materials Science and Engineering
Northwestern Polytechnical University
Xi'an, Shaanxi 710072, China
Dr. N. Liu, Prof. Y. Cui
Department of Materials Science and Engineering
Stanford University
Stanford, CA 94305, USA

DOI: 10.1002/aenm.201500214

Prof. A. R. Oganov
Department of Geosciences
State University of New York
Stony Brook, NY 11794-2100, USA
Prof. A. R. Oganov
Center for Materials by Design
Institute for Advanced Computational Science
State University of New York
Stony Brook, NY 11794-2100, USA
Prof. A. R. Oganov
Moscow Institute of Physics and Technology
9 Institutskiy Lane
Dolgoprudny City, Moscow Region 141700, Russian Federation
Prof. A. R. Oganov
International Center for Materials Discovery
Northwestern Polytechnical University
Xi'an, Shanxi 710072, China
Prof. Y. Cui, Prof. W. L. Mao
Photon Science and Stanford Institute for Materials
and Energy Sciences
SLAC National Accelerator Laboratory
Menlo Park, CA 94025, USA

to overcoming this challenge in the past decade.[17–19] One effective approach is to improve the mechanical performance of Si anodes by coating with stiffer materials, or by using Si-alloys and Si–C composites.[20,21] Improvement of the mechanical properties of Li–Si compounds (e.g., $Li_{15}Si_4$), however, has not yet been achieved. Pressure (compressive stress) has been found to remarkably alter the properties and structure of both Li and Si, the two end members of the Li–Si system, e.g., pressure-induced metal-to-insulator and solid–liquid (so-called "cold melting") transitions in Li, and pressure-induced semiconductor-to-metal and low-density to high-density polyamorphic transitions in Si.[22–25] For the Li–Si binary system, a stable compound LiSi was synthesized at a pressure of 1.0–2.5 GPa and 500–700 °C, which has never been observed under ambient conditions.[26,27] However, the effect of pressure on the structure and properties of $Li_{15}Si_4$ remains elusive.

In this study, we combined in situ high-pressure synchrotron XRD and high-pressure Raman spectroscopy with ab initio evolutionary metadynamics calculations to investigate the structural and properties change of $Li_{15}Si_4$ up to 18 GPa. A new orthorhombic phase (β-$Li_{15}Si_4$) was discovered when $Li_{15}Si_4$ was compressed to above 7 GPa. This new β-$Li_{15}Si_4$ phase has substantially larger elastic moduli compared with the original cubic phase, and can be recovered under ambient conditions, opening up opportunities for applications. These results improve our understanding of the Li–Si system under stress, and may provide guidance for improved electrode design.

2. Results and Discussion

2.1. Pressure-Induced Phase Transition

The structure of the as-prepared $Li_{15}Si_4$ was characterized at ambient pressure (0 GPa) in a sealed DAC prior to gas loading, confirmed to be single-phase polycrystalline $Li_{15}Si_4$ (space group $I\bar{4}3d$). The Rietveld full-profile refinement of the XRD pattern was performed using the GSAS program and EXPGUI package,[28] and the results are shown in Figure S1 and Table S1 in the Supporting Information. Angle-dispersive XRD was conducted under compression up to 18.0 GPa, followed by decompression to ambient pressure. XRD patterns during the compression and decompression are shown in **Figure 1**a. The original cubic structure remains stable up to 5.8 GPa upon pressure increasing. A new peak between (211) and (220) reflections starts to emerge at 7.1 GPa, indicating the formation of a new phase coexisting with the original cubic phase. This peak grows along with the increasing pressure, implying a sluggish phase transition. Other peaks for the new phase cannot be well resolved since they severely overlap with the peaks of the cubic phase. But, the transition is still observable due to the significant change in intensity of peaks.

At 18.0 GPa, the intense Bragg peaks (332) and (431) of the cubic phase completely disappear, whereas (220), (310), and (422) reflections seem to persist. The *d*-spacings associated with these three reflections are plotted as a function of pressure in **Figure 2**. The *d*-spacings shrink continuously as a result of lattice compression. A third-order Birch–Murnaghan equation of state[7] fits the low pressure data (below 7 GPa) very well. The deviation shown above 7 GPa indicates that the structural transition is beginning to occur. This is consistent with the pressure at which the new peak is observed (7.1 GPa). The new phase and the original cubic phase coexist over a wide pressure range from 7.1 GPa to 15.0 GPa. At 18.0 GPa, little residual cubic phase is present, and the diffraction pattern mainly corresponds to the new phase. The Bragg peaks for the new phase show substantial broadening compared with the original phase. This is also clearly seen in the unrolled 2D diffraction images of the two phases at 18.0 GPa and 0.9 GPa, respectively (see Figure 1b). The peak broadening may be attributed to reduced grain size or poor crystallinity in the high-pressure phase. Deviatoric stress may also contribute to the peak width increase,

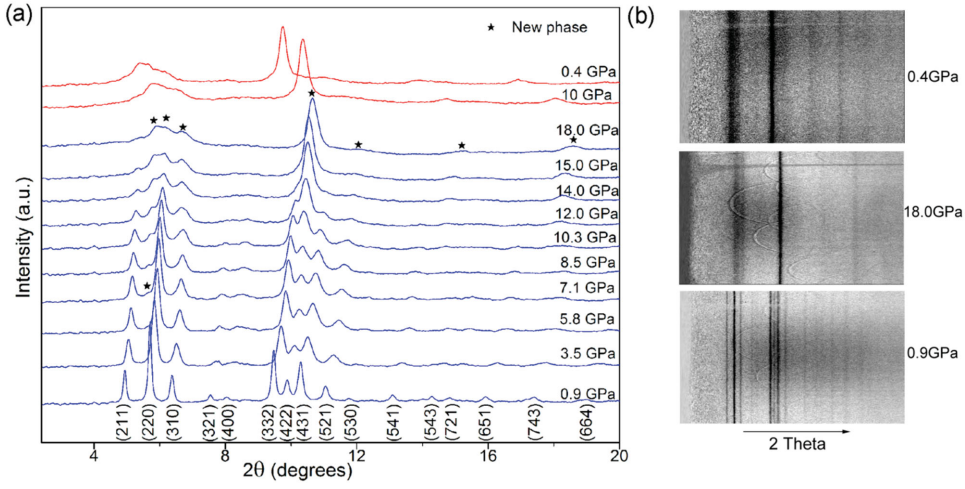

Figure 1. a) In situ high-pressure XRD patterns for crystalline $Li_{15}Si_4$ during compression up to 18.0 GPa and decompression to 0.4 GPa at room temperature ($\lambda = 0.3738$ Å). The Miller indices for the XRD pattern collected at 0.9 GPa are listed at the bottom. The diffraction peaks for the new phase are marked by stars. b) Unrolled 2D diffraction image of $Li_{15}Si_4$ at 0.9 GPa and 18.0 GPa during compression and at 0.4 GPa during decompression. Background scattering from the diamond anvils has been subtracted.

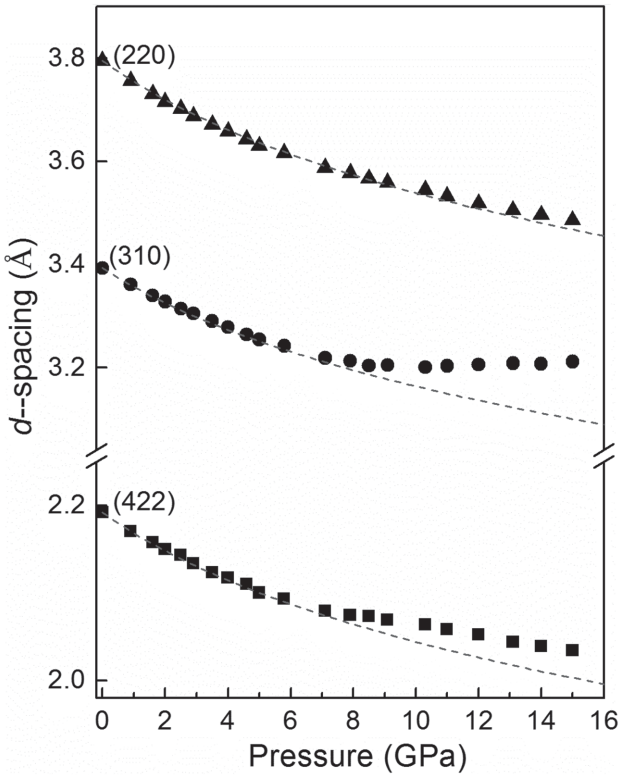

Figure 2. The pressure dependence of the *d*-spacing associated with Bragg peaks (422) (squares), (310) (circles), and (220) (triangles). The blue dashed lines are fit of the *d*-spacings using the equation of state for cubic $Li_{15}Si_4$ obtained in a previous study.[7]

but in this work the effect should be minor as helium provides a very hydrostatic environment over the pressure range of this experiment. In addition, the Bragg peak width does not change markedly after decompression to 0.4 GPa.

During decompression, the new phase is retained to ambient pressure. The lowest pressure shown in Figure 1 is 0.4 GPa because the sample reacted instantly with the air leaked in upon full decompression. In repeated high-pressure XRD experiments, the new phase remains stable up to the highest pressure studied (30.9 GPa). These results demonstrate that this new phase can be retained over a wide pressure range. The successful recovery of this new phase to ambient pressure suggests that it is also a metastable phase under ambient conditions analogous to cubic $Li_{15}Si_4$. This would enable us to study the properties and explore possible applications of this new phase under ambient conditions in the future.

2.2. Crystal Structure of the New $Li_{15}Si_4$ Phase

With the high brightness of the third-generation synchrotron radiation X-ray source at APS and background scattering subtraction, clear XRD patterns were obtained from the $Li_{15}Si_4$ sample despite its low scattering ability. However, solving the crystal structure of the new $Li_{15}Si_4$ phase from the XRD data was difficult due to the relatively weak diffraction pattern, broadening of the peaks, together with the few reflections

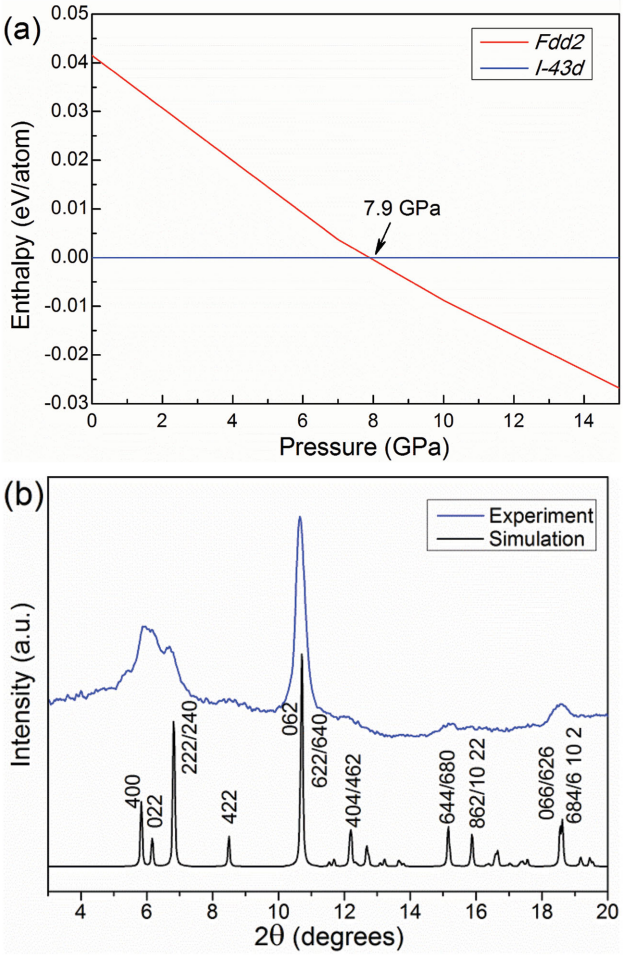

Figure 3. a) The enthalpy difference between orthorhombic *Fdd2* and cubic $I\bar{4}3d$ phases of $Li_{15}Si_4$ as a function of pressure. b) The calculated XRD pattern for the new orthorhombic structure at 18.0 GPa (black curve). The experimental XRD pattern for the $Li_{15}Si_4$ at the same pressure (blue curve) is plotted as a comparison.

observed and large unit cell of the original phase. Conventional theoretical prediction of the structure is challenging, given the large unit cell (76 atoms per unit cell) and metastability of the starting phase. Therefore, a new evolutionary metadynamics method was employed to predict the structure of high-pressure phase of $Li_{15}Si_4$. This technique is efficient for systems with large unit cells. Herein, the atomic structure for cubic $Li_{15}Si_4$ was used as a starting point to search for energetically favorable phases under high pressure. A novel orthorhombic structure (space group: *Fdd2* (No. 43)), which has a lower enthalpy than the cubic phase under pressure, was discovered. The enthalpies of both structures as a function of pressure were calculated, and their difference is shown in **Figure 3**a. The orthorhombic phase has a lower enthalpy at pressures above 7.9 GPa. This transition pressure agrees well with the transition pressure observed in the XRD experiment (7.1 GPa).

The calculated XRD pattern for the new phase at 18.0 GPa is plotted along with the experimental data at the same pressure for comparison (see Figure 3b). The peak positions in the calculated and the experimental XRD patterns are consistent.

Table 1. Fractional atomic coordinates for the new phase of $Li_{15}Si_4$ (*Fdd2*, $Z = 8$, $T = 0$ K, $P = 0$ GPa).

Atom	Wyckoff position	*x*	*y*	*z*	Occupancy
Si1	16b	0.62867	0.58276	0.37062	1.00
Si2	16b	0.62332	0.58309	0.86893	1.00
Li3	16b	0.29461	0.58336	0.36518	1.00
Li4	16b	0.71128	0.49702	0.62173	1.00
Li5	16b	0.42389	0.50012	0.61927	1.00
Li6	16b	0.45395	0.58590	0.86502	1.00
Li7	16b	0.45054	0.33352	0.12560	1.00
Li8	16b	0.85999	0.50093	0.62020	1.00
Li9	16b	0.54708	0.41793	0.36682	1.00
Li10	8a	0.50000	1.00000	0.10284	1.00

The relative intensity of the peaks in the calculated XRD pattern is also consistent with the experimental data, except in the $4° < 2\theta < 8°$ region. This could be attributed to the residual cubic phase in the experiment. According to the calculation, the new phase has a space group of *Fdd2* (No. 43) and 152 atoms in the conventional cell, twice as that in the cubic phase. The lattice parameters of the new phase (*Fdd2*-$Li_{15}Si_4$) are $a = 15.9075$ Å, $b = 14.7123$ Å, and $c = 8.4981$ Å at ambient pressure. **Table 1** provides the atomic positions and occupancy in the unit cell. Due to the complicated atomic structure and relatively low symmetry of the new phase, and the broad weak peaks observed in its XRD patterns, Rietveld refinement of the experimental XRD patterns is rather challenging.

The schematic diagrams in **Figure 4** depict the crystal structures of $I\bar{4}3d$ -$Li_{15}Si_4$ (α-$Li_{15}Si_4$) and *Fdd2*-$Li_{15}Si_4$ (β-$Li_{15}Si_4$) at ambient pressure. Unlike other Li–Si compounds with lower Li content that contain Si-Si bonds, in α-$Li_{15}Si_4$, Si atoms are exclusively coordinated by Li atoms. Therefore, its crystal structure can be considered packing of Si-centered $SiLi_n$ polyhedra, as shown in Figure 4c,d. All the Si atoms in the unit cell are equivalent, and each Si atom is 12-coordinate. The β-$Li_{15}Si_4$ is also composed of Si-centered $SiLi_n$ polyhedra, as shown in Figure 4a,b. But, in this phase Si atoms occupy two symmetry-independent positions Si1 and Si2. This leads to two types of $SiLi_n$ polyhedra with coordination numbers (CN) of 12 and 13, respectively (see Figure 4a). The location of these two types of polyhedra in the unit cell is shown in Figure 4b. The average coordination number of Si atoms (CN = 12.5) in β-$Li_{15}Si_4$ is higher than that in α-$Li_{15}Si_4$ (CN = 12). In Si1 polyhedra the shortest Si–Li bonds range from 2.465 to 2.806 Å (average bond length 2.689 Å), and in Si2 polyhedra the range is 2.482–2.824 Å (average bond length 2.708 Å). Both are shorter than the nearest Si–Li distance in α-$Li_{15}Si_4$ (2.605–2.867 Å, average bond length 2.765 Å).[14] The higher coordination number and shorter Si–Li bonds in β-$Li_{15}Si_4$ suggest that atoms in this phase are packed more efficiently than in α-$Li_{15}Si_4$, which is consistent with the much higher density of β-$Li_{15}Si_4$ (1.446 g cm^{-3}, 22% higher than that of α-$Li_{15}Si_4$ at ambient pressure). This is comparable with the diamond cubic→β–tin phase transition in Si, which is accompanied by an increase in coordination number from 4 to 6 and a volume decrease (density increase) of 21%.[24]

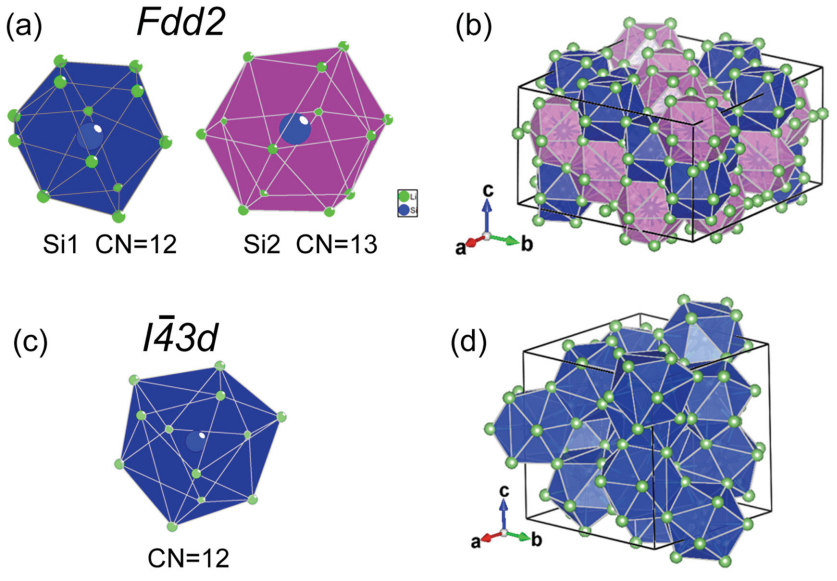

Figure 4. Schematic diagram indicating crystal structure of the two $Li_{15}Si_4$ phases: a) two types of Si-centered polyhedra in *Fdd2* phase with coordination number CN = 12 (blue) and CN = 13 (pink), b) the arrangement of the polyhedra in the conventional unit cell of *Fdd2*, c) Si-centered polyhedra, and d) the arrangement of polyhedra in the $I\bar{4}3d$ phase (green: Li; blue: Si)

2.3. Properties of the New $Li_{15}Si_4$ Phase

Knowledge of the electrical conductivity and mechanical properties is essential for lithium-ion battery electrode materials. As a result, the properties of α-$Li_{15}Si_4$ and other Li–Si compounds have been studied extensively. First-principles calculations suggest that the bandgap of Li–Si compounds gradually diminishes with increasing Li content, and that α-$Li_{15}Si_4$ is a metal or a narrow gap semiconductor.[4,29] For comparison, we calcu-

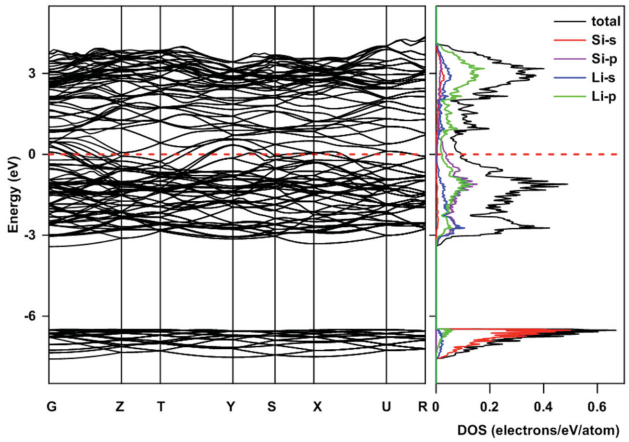

Figure 5. Electronic band structure (left), density of states (DOS), and its projection onto atomic orbitals (right) for β-$Li_{15}Si_4$.

lated the band structure and electronic density of states (DOS) of β-$Li_{15}Si_4$ (see **Figure 5**). The results suggest that β-$Li_{15}Si_4$ is a metal as α-$Li_{15}Si_4$.[30] In addition, the total DOS of β-$Li_{15}Si_4$ shows a dip above the Fermi level; a similar dip is also observed in DOS of α-$Li_{15}Si_4$.[6,30] These results indicate that the electrical properties of $Li_{15}Si_4$ are not sensitive to the changes in atomic structure such as Si–Li bond length and Si–Li coordination number.

The metallic behavior of β-$Li_{15}Si_4$ is also supported by the results of high-pressure Raman spectroscopy experiment. Raman spectra of $Li_{15}Si_4$ were collected during compression to 18.0 GPa and decompression to 2.9 GPa. At the starting pressure (1.3 GPa), α-$Li_{15}Si_4$ does not show a visible Raman band in the range of 100–1000 cm^{-1} (see **Figure 6**). No Raman peaks can be observed up to 18.0 GPa, during which α-$Li_{15}Si_4$ transforms to β-$Li_{15}Si_4$ according to the XRD results. Furthermore, no Raman bands emerge during decompression when β-$Li_{15}Si_4$ is recovered to lower pressure (2.9 GPa). These results suggest β-$Li_{15}Si_4$ has a very weak Raman signal that cannot be observed under current experimental conditions. Since Raman bands for metals are usually extreme weak as a result of the weak scattering due to the high reflectivity, the lack of noticeable Raman

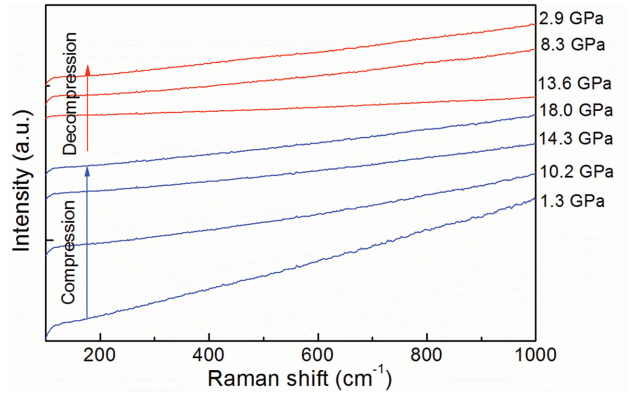

Figure 6. In situ high-pressure Raman spectrum for $Li_{15}Si_4$ during compression up to 18.0 GPa (blue curves) and decompression to 2.9 GPa (red curves) at room temperature.

peaks in β-$Li_{15}Si_4$ is consistent with the metallic property predicted by our calculations.

We also studied the mechanical properties of $Li_{15}Si_4$ after the phase transition. The elastic moduli and Poisson's ratio of polycrystalline β-$Li_{15}Si_4$ and α-$Li_{15}Si_4$ are compared in **Table 2**. β-$Li_{15}Si_4$ has substantially enhanced mechanical properties with higher bulk, Young's, and shear moduli, which means that it is a stiffer phase than α-$Li_{15}Si_4$. The elastic moduli of Li–Si compounds are found to depend strongly on Li concentration and show significant softening in Li-rich phases.[5] α-$Li_{15}Si_4$ with its high Li content is a very soft material because of the decreased connectivity in the Si framework. Compared with the three-fold-coordinated Si atoms in LiSi and Si_2 dumbbells in $Li_{13}Si_4$,[27] all the Si atoms in α-$Li_{15}Si_4$ are isolated. In β-$Li_{15}Si_4$ the Si atoms are isolated as well; thus, the enhanced mechanical properties in β- $Li_{15}Si_4$ do not originate from the formation of Si-Si bonds. Instead, shorter Li–Si and Li–Li bonds in β-$Li_{15}Si_4$ may explain its enhanced elastic moduli.

The relatively higher density of β-$Li_{15}Si_4$ results in a lower theoretical volume expansion of Si. The theoretical volume expansion of Si during lithiation is widely accepted as 280%, where Si is considered to totally transform to α-$Li_{15}Si_4$ that leads to a 280% volume increase. This value would be reduced to 210% if Si transformed to β-$Li_{15}Si_4$ during lithiation, which is calculated according to its density. The significantly higher Young's and shear modulus indicate higher resistance to normal and shear stress, which remarkably reduce the deformation and fracture of $Li_{15}Si_4$ under stress. These improvements in the properties of $Li_{15}Si_4$ associated with the $\alpha \rightarrow \beta$ phase transition may provide a new perspective to optimize Si-based anode materials. Although in this study β-$Li_{15}Si_4$ was synthesized by applying external pressure, doping with impurities has been proven to be an efficient approach for changing the thermodynamic stability of α-$Li_{15}Si_4$.[14] Chemical pressure induced by doping might facilitate the formation of β-$Li_{15}Si_4$ phase at ambient conditions.

3. Conclusion

In summary, we studied the behavior of $Li_{15}Si_4$ under pressure by using in situ high-pressure synchrotron XRD, high-pressure Raman spectroscopy coupled with ab initio evolutionary algorithm calculations. A new β-$Li_{15}Si_4$ phase was discovered when pressure reaches 7 GPa, and this sluggish phase transition was almost complete at 18.0 GPa. This new phase of $Li_{15}Si_4$ has a space group of *Fdd2* (No. 43) and 152 atoms per unit cell, and can be retained under ambient conditions. β-$Li_{15}Si_4$ is as good a conductor of electrons as α-$Li_{15}Si_4$ and shows substantially improved mechanical properties. These results deepen our understanding of $Li_{15}Si_4$ and the Li–Si system, and will also

Table 2. Elastic moduli and Poisson's ratio for α- and β-$Li_{15}Si_4$ phases.

Phase	Bulk modulus [GPa]	Young's modulus [GPa]	Shear modulus [GPa]	Poisson's ratio
$I\bar{4}3d$	28.4[7], 30.2[5]	50[5]	4[7], 21[5]	0.43[7], 0.23[5]
Fdd2	35.6	79.6	35.3	0.13

stimulate future study of the novel β-$Li_{15}Si_4$ phase for optimizing Si as an anode material.

4. Experimental Section

Material Synthesis: The crystalline $Li_{15}Si_4$ sample in our work was synthesized in a Li battery by electrochemical lithiation of a Si wafer (50 μm thick). Li batteries (2032-type coin cell) were prepared inside an Ar-filled glovebox using a Si wafer as the working electrode, Li metal as the counter electrode, and a Celgard separator soaked in an electrolyte. The electrolyte was 1.0 M $LiPF_6$ in 1:1 (w/w) ethylene carbonate/diethyl carbonate (EMD Chemicals). For lithiation of the Si wafer, a linear sweep voltammetry was carried out using a Bio-logic VMP3 battery tester. The battery was lithiated to a voltage of 5 mV versus Li/Li^+ from the open circuit voltage at 2 mV s^{-1} and held at this voltage for about 40 h to ensure complete lithiation. The formed $Li_{15}Si_4$ was retrieved by disassembling the coin cell and washing with anhydrous diethyl carbonate. Due to the high reactivity of $Li_{15}Si_4$ in air, the $Li_{15}Si_4$ was carefully handled and not exposed to air throughout the whole process. Typical electrochemical data of the batteries can be found in a previous paper.[7]

In Situ High-Pressure XRD and Raman Spectroscopy Experiments: The $Li_{15}Si_4$ sample was loaded into a symmetric diamond anvil cell (DAC) in an Ar-filled glovebox for high-pressure experiments. Two tiny ruby balls were loaded along with each sample as a pressure calibrant. Pressure was measured in situ by monitoring the shift in the R1 fluorescence line of ruby.[31] The sample chamber was a 150 μm diameter hole drilled in a T301 stainless-steel gasket, which is inert with respect to $Li_{15}Si_4$. After sample loading, the DAC was sealed before the removal from the glovebox. Helium was then loaded into the sample chamber as the hydrostatic pressure transmitting medium using the high-pressure gas loading system at GSECARS, Advanced Photon Source (APS), Argonne National Laboratory (ANL). In situ high-pressure angle-dispersive XRD experiments were performed with a focused X-ray beam of 15×15 μm^2 (FWHM) at a wavelength of 0.3738 Å, at beamline 16 ID-B of the High Pressure Collaborative Access Team (HPCAT), APS, ANL. A MAR165 CCD detector was used for data collection, and the software package FIT2D was used to integrate the Debye–Scherrer rings.[32] Background scattering was obtained by collecting XRD patterns through the same DAC and gasket with sample removed. In situ high-pressure Raman measurements were carried out using a Renishaw inVia micro Raman system with a 514 nm laser excitation line. A low laser power of 2.5 mW was used to minimize any thermal effects, with a collection time of 180 s for each measurement. The sample was confirmed to be pure $Li_{15}Si_4$ by synchrotron XRD before the Raman measurements. The DAC not only generated high pressure, but also provided an ideal airtight sample chamber for the chemically reactive $Li_{15}Si_4$ samples with X-ray and optical laser transparent diamond windows.

Computational Methodology: It was crucial to first determine the structure of a compound before its properties can be further investigated. Due to the large number of atoms, four formula units of α-$Li_{15}Si_4$ in its unit cell, it was very difficult to find the structure of the new phase of $Li_{15}Si_4$. Furthermore, α-$Li_{15}Si_4$ is a metastable phase and its room-temperature transformation into β-$Li_{15}Si_4$ is likely to be also metastable. For finding the most likely metastable phase transitions from a given starting phase, using an evolutionary metadynamics algorithm is optimal—furthermore, it easily handled large systems. Evolutionary metadynamics explores the free energy surface, combining gradual deformation of the unit cell with large atomic displacements along the eigenvectors of a number of softest vibrational modes. The latter allowed us to map all low-barrier transformations, enabling the prediction of the most likely metastable phase transitions. Starting from a reasonable initial structure, this method is capable of also efficiently discovering the global energy minimum. A detailed description of this method can be found in ref. [33], and its application to metastable carbon is presented in ref. [34]. This method was implemented in the USPEX code,[35–37] which we used in this work. Structure relaxations were conducted using density functional theory (DFT) within the generalized gradient approximation (GGA)[38] in the framework of the all-electron projector augmented wave (PAW)[39] method as implemented in the VASP code.[40] A plane-wave kinetic energy cutoff of 340 eV for the plane-wave basis set and a Brillouin zone sampling resolution $2\pi \times 0.06$ $Å^{-1}$ were used. Starting from the $I\bar{4}3d$ phase, at the pressure of 10 GPa its transformation into a more stable *Fdd2* structure was quite easily found, which matched all experimental results and was proposed to be the structure of β-$Li_{15}Si_4$.

A larger energy cutoff of 520 eV and denser k-point meshes with the reciprocal space resolution of $2\pi \times 0.04$ $Å^{-1}$ were used for further calculations of physical properties. The calculations of the elastic properties, band structure, and density of states (DOS) of β-$Li_{15}Si_4$ were done using the VASP code. The elastic constants were calculated from the stress–strain relations, and the Voigt–Reuss–Hill (VRH) approximation was employed to obtain the bulk modulus, shear modulus, Young's modulus, and Poisson's ratio of β-$Li_{15}Si_4$ at ambient pressure.[41,42]

Supporting Information

Supporting Information is available from the Wiley Online Library or from the author.

Acknowledgements

Z.Z. and Q.F.Z. contributed equally to this work. The authors thank Dr. Jiyong Zhao, Yang Ding, Stanislav V. Sinogeikin, and Sergey N. Tkachev for their kind help with their experiments. This work of W.L.M. was supported by the Department of Energy, Office of Science, Basic Energy Sciences, Materials Sciences and Engineering Division, under Contract No. DE-AC02-76SF00515. The experiments were performed at HPCAT (Sector 16), APS, ANL, and 12.2.2, ALS. HPCAT operations are supported by CIW, CDAC, UNLV, and LLNL through funding from DOE-NNSA and DOE-BES, with partial instrumentation funding by NSF. APS was supported by DOE-BES, under Contract No. DE-AC02-06CH11357. ALS was supported by DOE-BES, under Contract No. DE-AC02-05CH11231. Use of the gas loading system at GSECARS was supported by NSF (EAR-0622171, EAR 06-49658, and EAR 10-43050), DOE (DE-FG02-94ER14466), and COMPRES. Q.F.Z. acknowledges the support from the National Natural Science Foundation of China (Nos. 51372203 and 11372260), and the High Performance Computing Center of NWPU for the allocation of computing time on their machines. A.R.O. thanks the National Science Foundation (EAR-1114313, DMR-1231586), DARPA (Grant Nos. W31P4Q1210008 and W31P4Q1310005), the Government (Grant No. 14.A12.31.0003) of Russian Federation, and Foreign Talents Introduction and Academic Exchange Program (No. B08040). Y.C. acknowledges the support from the Assistant Secretary for Energy Efficiency and Renewable Energy, Office of Vehicle Technologies of the U.S. Department of Energy under Contract No. DE-AC02-05CH11231, Subcontract No. 6951379 under the Batteries for Advanced Transportation Technologies (BATT) Program.

Received: January 29, 2015
Revised: March 13, 2015
Published online:

[1] B. A. Boukamp, G. C. Lesh, R. A. Huggins, *J. Electrochem. Soc.* **1981**, *128*, 725.
[2] C. K. Chan, H. L. Peng, G. Liu, K. McIlwrath, X. F. Zhang, R. A. Huggins, Y. Cui, *Nat. Nanotechnol.* **2008**, *3*, 31.
[3] M. Zeilinger, D. Benson, U. Haussermann, T. F. Fassler, *Chem. Mater.* **2013**, *25*, 1960.

[4] M. Zeilinger, I. M. Kurylyshyn, U. Haussermann, T. F. Fassler, *Chem. Mater.* **2013**, *25*, 4623.
[5] V. B. Shenoy, P. Johari, Y. Qi, *J. Power Sources* **2010**, *195*, 6825.
[6] V. L. Chevrier, J. W. Zwanziger, J. R. Dahn, *J. Alloys Compd.* **2010**, *496*, 25.
[7] Z. Zeng, N. Liu, Q. Zeng, Y. Ding, S. Qu, Y. Cui, W. L. Mao, *J. Power Sources* **2013**, *242*, 732.
[8] M. K. Y. Chan, C. Wolverton, J. P. Greeley, *J. Am. Chem. Soc.* **2012**, *134*, 14362.
[9] B. Key, M. Morcrette, J.-M. Tarascon, C. P. Grey, *J. Am. Chem. Soc.* **2011**, *133*, 503.
[10] J. Zhao, Z. Lu, N. Liu, H.-W. Lee, M. T. McDowell, Y. Cui, *Nat. Commun.* **2014**, *5*.
[11] J. E. Cloud, Y. Wang, T. S. Yoder, L. W. Taylor, Y. Yang, *Angew. Chem. Int. Ed.* **2014**, *53*, 14527.
[12] J. Li, J. R. Dahn, *J. Electrochem. Soc.* **2007**, *154*, A156.
[13] S. Misra, N. Liu, J. Nelson, S. S. Hong, Y. Cui, M. F. Toney, *ACS Nano* **2012**, *6*, 5465.
[14] M. Zeilinger, V. Baran, L. van Wullen, U. Haussermann, T. F. Fassler, *Chem. Mater.* **2013**, *25*, 4113.
[15] H. Kim, C. Y. Chou, J. G. Ekerdt, G. S. Hwang, *J. Phys. Chem. C* **2011**, *115*, 2514.
[16] M. J. Chon, V. A. Sethuraman, A. McCormick, V. Srinivasan, P. R. Guduru, *Phys. Rev. Lett.* **2011**, *107*, 045503.
[17] A. Mukhopadhyay, B. W. Sheldon, *Prog. Mater. Sci.* **2014**, *63*, 58.
[18] M. T. McDowell, S. W. Lee, W. D. Nix, Y. Cui, *Adv. Mater.* **2013**, *25*, 4966.
[19] H. Wu, G. Chan, J. W. Choi, I. Ryu, Y. Yao, M. T. McDowell, S. W. Lee, A. Jackson, Y. Yang, L. Hu, Y. Cui, *Nat. Nanotechnol.* **2012**, *7*, 310.
[20] H. Li, X. J. Huang, L. Q. Chen, Z. G. Wu, Y. Liang, *Electrochem. Solid-State Lett.* **1999**, *2*, 547.
[21] Y. He, X. Q. Yu, Y. H. Wang, H. Li, X. J. Huang, *Adv. Mater.* **2011**, *23*, 4938.
[22] C. L. Guillaume, E. Gregoryanz, O. Degtyareva, M. I. McMahon, M. Hanfland, S. Evans, M. Guthrie, S. V. Sinogeikin, H. K. Mao, *Nat. Phys.* **2011**, *7*, 211.
[23] T. Matsuoka, K. Shimizu, *Nature* **2009**, *458*, 186.
[24] J. C. Jamieson, *Science* **1963**, *139*, 762.
[25] S. K. Deb, M. Wilding, M. Somayazulu, P. F. McMillan, *Nature* **2001**, *414*, 528.
[26] J. Evers, G. Oehlinger, G. Sextl, *Angew. Chem. Int. Ed.* **1993**, *32*, 1442.
[27] L. A. Stearns, J. Gryko, J. Diefenbacher, G. K. Ramachandran, P. F. McMillan, *J. Solid State Chem.* **2003**, *173*, 251.
[28] B. H. Toby, *J. Appl. Cryst.* **2001**, *34*, 210.
[29] C. A. Bridges, X.-G. Sun, J. Zhao, M. P. Paranthaman, S. Dai, *J. Phys. Chem. C* **2012**, *116*, 7701.
[30] Y. H. Xu, G. P. Yin, P. J. Zuo, *Electrochim. Acta* **2008**, *54*, 341.
[31] H. K. Mao, P. M. Bell, J. W. Shaner, D. J. Steinberg, *J. Appl. Phys.* **1978**, *49*, 3276.
[32] A. P. Hammersley, S. O. Svensson, M. Hanfland, A. N. Fitch, D. Hausermann, *High Pres. Res.* **1996**, *14*, 235.
[33] Q. Zhu, A. R. Oganov, A. O. Lyakhov, *Cryst. Eng. Commun.* **2012**, *14*, 3596.
[34] Q. Zhu, Q. Zeng, A. R. Oganov, *Phys. Rev. B: Condens. Matter* **2012**, *85*, 201407.
[35] A. O. Lyakhov, A. R. Oganov, H. T. Stokes, Q. Zhu, *Comp. Phys. Commun.* **2013**, *184*, 1172.
[36] A. R. Oganov, C. W. Glass, *J. Chem. Phys.* **2006**, *124*.
[37] A. R. Oganov, A. O. Lyakhov, M. Valle, *Acc. Chem. Res.* **2011**, *44*, 227.
[38] J. P. Perdew, K. Burke, M. Ernzerhof, *Phys. Rev. Lett.* **1996**, *77*, 3865.
[39] P. E. Blochl, *Phys. Rev. B: Condens. Matter* **1994**, *50*, 17953.
[40] G. Kresse, J. Furthmuller, *Phys. Rev. B: Condens. Matter* **1996**, *54*, 11169.
[41] R. Hill, *Proc. Phys. Soc. London A* **1952**, *65*, 349.
[42] A. Reuss, Z. Angnew, *Math. Met.* **1929**, *9*, 55.